Electron Linac design to drive bright Compton back-scattering gamma-ray sources

A. Bacci, D. Alesini, P. Antici, M. Bellaveglia, R. Boni et al.

Citation: J. Appl. Phys. **113**, 194508 (2013); doi: 10.1063/1.4805071
View online: http://dx.doi.org/10.1063/1.4805071
View Table of Contents: http://jap.aip.org/resource/1/JAPIAU/v113/i19
Published by the American Institute of Physics.

JOURNAL OF APPLIED PHYSICS **113**, 194508 (2013)

Electron Linac design to drive bright Compton back-scattering gamma-ray sources

A. Bacci,[1] D. Alesini,[2] P. Antici,[3] M. Bellaveglia,[2] R. Boni,[2] E. Chiadroni,[2] A. Cianchi,[4] C. Curatolo,[1,5] G. Di Pirro,[2] A. Esposito,[2] M. Ferrario,[2] A. Gallo,[2] G. Gatti,[2] A. Ghigo,[2] M. Migliorati,[3] A. Mostacci,[3] L. Palumbo,[3] V. Petrillo,[1,5] R. Pompili,[2,4] C. Ronsivalle,[6] A. R. Rossi,[1] L. Serafini,[1] B. Spataro,[2] P. Tomassini,[5] and C. Vaccarezza[2]
[1]*INFN-MI, Milano, Italy*
[2]*INFN-LNF, Frascati, Roma, Italy*
[3]*University La Sapienza, Roma, Italy*
[4]*University of Tor Vergata, Roma, Italy*
[5]*University of Milano, Milano, Italy*
[6]*Enea, Frascati, Roma, Italy*

(Received 29 January 2013; accepted 1 May 2013; published online 20 May 2013)

The technological development in the field of high brightness linear accelerators and high energy/high quality lasers enables today designing high brilliance Compton-X and Gamma-photon beams suitable for a wide range of applications in the innovative field of nuclear photonics. The challenging requirements of this kind of source comprise: tunable energy (1–20 MeV), very narrow bandwidth (0.3%), and high spectral density (10^4 photons/s/eV). We present here a study focused on the design and the optimization of an electron Linac aimed to meet the source specifications of the European Extreme Light Infrastructure—Nuclear Physics project, currently funded and seeking for an innovative machine design in order to outperform state-of-the-art facilities. We show that the phase space density of the electron beam, at the collision point against the laser pulse, is the main quality factor characterizing the Linac. © *2013 AIP Publishing LLC*. [http://dx.doi.org/10.1063/1.4805071]

I. INTRODUCTION

Advanced gamma-ray sources, based on Compton back-scattering between electron bunches and counter-propagating laser pulses, are considered to be the new road-map to open the field of nuclear photonics. Several laboratories world-wide are pursuing projects to develop such advanced Compton sources (Mega-ray project,[1] AIST[2]), with the main aim to step up from the present state of the art parameters, represented by the facility HIGS,[3] where nuclear physics experiments with mono-chromatic gamma ray beams are being performed for a few years by now. In particular, at the Nuclear Physics Pillar of the European laser facility ELI (Extreme Light Infrastructure), to be developed in Romania at Magurele (near Bucharest), an advanced Gamma System is foreseen as a major component of the infrastructure, aiming at producing extreme gamma ray beams for nuclear physics and nuclear photonics experiments for users. In this field, there are many strategic studies and applications for national security, nuclear waste treatment, nuclear medicine, and fundamental studies in nuclear physics, dealing with the nucleus structure and the role of giant dipole resonances, which will have an impact also on astrophysics and answer questions concerning star nucleosynthesis.

In this paper, we will describe a design for an electron Linac able to meet the challenging parameters of the gamma ray beam that Extreme Light Infrastructure-Nuclear Physics (ELI-NP) project is requiring. These parameters are briefly summarized in Table I, noticeably (1) the tunability of the mono-chromatic narrow bandwidth (0.3%) gamma ray beam in a wide range of energies, 1 to 20 MeV, to cover the range of Nuclear Resonance Fluorescence (NRF) experiments as well as giant resonance studies; (2) its extremely high spectral density (SPD) (up to 10^4 photons/eV/s, to be compared with about 10^3 photons/eV/s of present state of the art) and highly polarized state. As explained in the following sections, we are considering as best solution to use a room temperature hybrid S-band C-band electron Linac for applications where we need both average fluxes (hence average current) and peak performances (high phase space density, i.e., low emittance in a round beam with very small energy spread). Usually, these two requirements are conflicting, and a possible solution would be a super conducting (SC) energy recovery Linac (ERL): due to a short timeline and limited budget of the ELI-NP facility, the ERL solution was discarded. Therefore, we are concentrating on a high brightness normal conducting electron Linac (similar to those typically driving X-ray FELs) to produce high peak brightness in the single bunch as well as a multi-bunch beam with effective high repetition rate (rep. rate) to increase the average current.

Our proposed solution, illustrated in the following, is to run the Linac at the maximum radiofrequency (RF) rep. rate achievable (100 Hz), injecting from the photo-injectors into the booster Linac trains of bunches which are filling the available RF pulse time duration: typically, 32 bunches separated by 16 ns over a 512 ns flat RF pulse, leading to an effective rep. rate for the Linac of 3.2 kHz; this value is mainly imposed by the needed recirculation of the high intensity interaction laser, rather than RF pulse duration or other RF issues, which are beyond the scope of this paper.

TABLE I. Summary of gamma-ray beam specifications.

Photon energy	1–20 MeV
Spectral density	$>10^4$ ph/s eV
Bandwidth (rms)	≤0.3%
# photons per shot within FWHM bdw.	$2.0–4.0 \cdot 10^5$
# photons/s within FWHM bdw.	$\sim 10^9$
Source rms size	10–30 μm
Source rms divergence	25–250 μrad
Peak brilliance (N_{ph}/s·mm^2 mrad^2·0.1%)	10^{23}–10^{24}
Radiation pulse length (rms, ps)	0.7–1.5
Linear polarization	>95%
Macro rep. rate	100 Hz
# of pulses per macropulse	30–40
Pulse-to-pulse separation	15–20 ns

We find that a machine design based on the use of an RF Linac operated at C-band (5.7 GHz) with an S-band photo-injector similar to SPARC,[4] delivering a high phase space density electron beam in the 180–750 MeV energy range, colliding with a Yb:Yag high power laser (Table II), to produce via Compton back-scattering a gamma-ray photon beam, represents a possible option to satisfy the requirements of the ELI-NP gamma source. The electron beam characteristics are fundamental for these kind of sources. Normalized rms emittances in both planes below 0.5 mm-mrad are needed, such as energy spread below 0.1%. Noticeably, these rms beam quality factors have to be evaluated on projected (integrated) values over the electron bunch, unlike in FEL's machines where the so called "slice" values are mostly relevant for the high gain FEL process. In the following, the design criteria and the main characteristics of the accelerator are presented.

II. THE GAMMA-RAY COMPTON SOURCE

The classical model of the electron-photon interaction (Thomson scattering) has been studied extensively[5–8] and also verified by experiments.[9,10] The Compton model includes the quantum contribution and provides the final characteristics for a high energy source when the recoil of the electron cannot be disregarded.[11] Here, we describe this electron-photon interaction for the high energy case (E = 180–720 MeV), and the following formulas, starting from the luminosity concept Eq. (1), are useful scaling laws aimed to define the accelerator specifications. Their validity has been proven by simulation codes as shown in Ref. 11, codes used in start to end simulations in order to give the ELI-NP source characteristics (Table II).

TABLE II. Laser beam parameters.

Pulse energy (J)	0.5
Wavelength (eV)	2.48
FWHM pulse length (ps)	2–4
Repetition rate (Hz)	100
M^2	≤1.2
Focal spot size w_0 (μm)	>28
Bandwidth (rms)	0.05%
Pointing stability (μrad)	1
Sinchronization to an ext. clock	<1 ps
Pulse energy stability	1%

The typical geometry of the back-scattering between an electron bunch and a laser pulse is reported in Fig. 1. As in the case of colliders, we can define a luminosity parameter

$$L = \frac{N_L N_e}{2\pi(\sigma_x^2 + w_0^2/4)} f, \tag{1}$$

where N_L is the optical photons number of the laser pulse, N_e is the electrons number per bunch, σ_x is the rms electron bunch spot size (considering a round beam), and f is the collision rep. rate, obtained multiplying the RF rep. rate for the number of electron bunches into the RF pulse. Equation (1) is valid under the assumption of an optimal space-time overlapping of the two beams into the focal region, with a minimized hour-glass effect at the collision. This means that for the laser pulse transverse size at the waist ($w_0 = \sqrt{Z_r \lambda_L/\pi}$), and for the electron beam, have to hold: $w_0 \cong 2\sigma_x$, $cT < 2Z_r$, and $\sigma_z < \beta^* \equiv \gamma\sigma_x^2/\epsilon_{x,n}$, where β^* is the β Twiss parameter at the focus, $\epsilon_{x,n}$ is the normalized transverse emittance, and γ is the relativistic factor.

The total number of laser scattered photons is given by $N_\gamma = L \cdot \sigma_{th}$, where the Thomson cross-section is $\sigma_{th} = 0.67 \cdot 10^{-28}$ m^2. The ELI-NP project requires laser energy $U_L = 0.5$ J, laser photon energy $h\upsilon_L = 2.48$ eV, electron bunch charge $Q_b = 250$ pC, and, for example, spot size of $\sigma_x = 30$ μm for the electron beam and $w_0 = 60$ μm for the laser beam. In this case, the photon/second emitted over the whole solid angle is about $N_\gamma = 3.5 \times 10^{10}$ (considering a collision rep. rate of $f = 3 \times 10^3$).

The frequency ν_γ of the emitted radiation (single electron-photon interaction is reported in Ref. 11) within a small angle of scattering with respect to the propagation axes of the electron beam, in the case of head-on collision, is

$$\nu_\gamma \cong \nu_L \frac{4\gamma^2}{1 + \gamma^2\theta^2 + \frac{a_0^2}{2}}(1 - \Delta), \tag{2}$$

where θ is the observer angle, $a_0 = 4.3 \frac{\lambda_L}{w_0}\sqrt{\frac{U[J]}{\sigma_{t,L}[ps]}}$ is the laser parameter, and the dimensionless parameter $\Delta \cong \frac{4\gamma h\nu_L}{mc^2}$ (Refs. 11 and 12) takes into account the red-shift due to the electron recoil. For example, the collision between an electron beam at 720 MeV and a 0.5 J, 500 nm laser pulse, focused down to 15 μm ($a_0 = \sim 0.04$) along the electron direction of

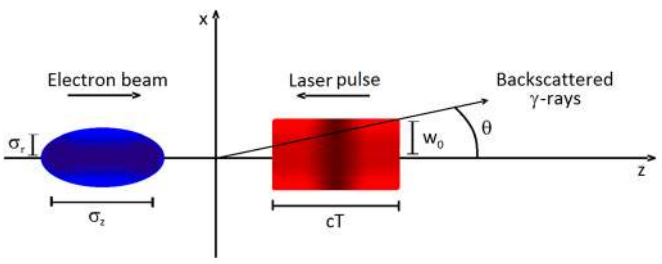

FIG. 1. Typical back scattering geometry between an electron bunch of longitudinal size σ_L and transversal size σ_R, moving at relativistic speed from left to right colliding with a laser pulse of waist size w_0 and time duration T.

propagation, generates 19.2 MeV gamma photons with a Compton recoil correction of about 0.53 MeV.

One of the most stringent parameters of this source, determining its high quality, is a very narrow bandwidth, which depends on the normalized collecting angle $\Psi_{\rm rms} = (\gamma\theta)_{\rm rms}$, the electron bunch energy spread $\frac{\Delta\gamma}{\gamma}$, its normalized transverse emittance $\varepsilon_{\rm n}$ (transversally round beams are assumed) the relative laser pulse bandwidth $\frac{\Delta\nu_L}{\nu_L}$, the diffraction $\frac{M^2\lambda_L}{2\pi w_0}$, and the temporal profile $\frac{a_0^2/3}{1+a_0^2/2}$ broadening contribution. The rms source bandwidth can then be expressed as[6,11]

$$\frac{\Delta\upsilon_\gamma}{\upsilon_\gamma} = \sqrt{(\gamma\theta)_{\rm rms}{}^4 + \left(\frac{\Delta\gamma}{\gamma}\right)^2 + \left(\frac{\varepsilon_n}{\sigma_x}\right)^4 + \left(\frac{\Delta\upsilon_L}{\upsilon_L}\right)^2 + \left(\frac{M^2\lambda_L}{2\pi w_0}\right)^4 + \left(\frac{a_0^2/3}{1+a_0^2/2}\right)^2}. \tag{3}$$

Imposing a specific value for the bandwidth (0.3% for the ELI-NP project), the maximum collecting angle is univocally defined. The number of photons per second in the assigned bandwidth, as described in Ref. 13, is given by

$$N_\gamma^{bw} = \frac{4.1\times10^8 U_L[\mathrm{J}]Q_b[pC]\Psi^2}{h\upsilon_l[\mathrm{eV}]\left(\sigma_x^2[\mu\mathrm{m}] + \frac{W_0^2}{4}\right)}. \tag{4}$$

Considering the ELI-NP project parameters (Tables I and II), the equation gives about $N_\gamma^{bw} \sim 10^9$ ph/s. It is now possible to define the SPD as the ratio between the number of photons in the bandwidth and the rms value of the bandwidth itself

$$SPD \equiv \frac{N_\gamma^{bw}}{\sqrt{2\pi}h\Delta\upsilon_\gamma}, \tag{5}$$

which gives the figure of merit of the gamma source and for the above values gives 10^4 (photons/s/eV), about two orders of magnitude higher than the current state of the art.

III. ACCELERATOR DESIGN CRITERIA

In order to establish the accelerator design criteria, we draw from Eqs. (3) and (4) the electron beam contribution to the source's SPD (Eq. (5)), defining the following factor of merit for the electron beam:

$$\hat{\eta} = \frac{Q_b}{\sigma_x^2\left[\left(\frac{\Delta\gamma}{\gamma}\right)^2 + \left(\frac{\varepsilon_n}{\sigma_x}\right)^4\right]^{1/2}}\left[\frac{C}{m^2}\right], \tag{6}$$

which scales like the spectral density of the emitted radiation and must be maximized. Since in a photo-Linac injector, also delivering high brightness electron beams, longitudinal and transverse phase spaces are not strongly coupled (in particular when no relevant bunch compression is needed at low energy, as in present case), we can assume that the emittance can be minimized for a given bunch charge, independently from the bunch energy spread. The result is to split the Linac injector optimization in two steps, maximizing first the electron density into the transverse phase space η

$$\eta \equiv \frac{Q_b}{\varepsilon_n{}^2}, \tag{7}$$

obtained from Eq. (6) disregarding the $\frac{\Delta\gamma}{\gamma}$ factor, then considering the energy spread constraint. The η value is strongly dependent from the electron source, in terms of RF, gun design, extraction laser spatial dimensions, and emittance compensation solenoid. Once the η is optimized, some flexibility remains for the $\frac{\Delta\gamma}{\gamma}$, which can be controlled by a light longitudinal bunch compression, in the first acceleration section, as explained in the following text.

The η maximization has been performed by an extensive campaign of numerical based optimizations[12] by using GIOTTO, a Genetic Algorithm code,[14,15] which is an *ad hoc* method for optimizing more conflicting objectives subject to certain constraints. Fig. 2 shows the phase space density (η) versus bunch charge as computed by GIOTTO, for different frequency bands and assuming to consider state of the art of the peak field on the cathode for each frequency: each curve is the result of the genetic algorithm optimization carried out over hundreds of single runs spanning the operating range of dynamical free parameters. The results obtained from these simulations, in terms of η, are in agreement with the published S-band measured best values.[16,17]

Though both simulations and experimental results (LCLS[16,17]) show high η values, these values are non-compatible with the ELI-NP electron beam energy spread

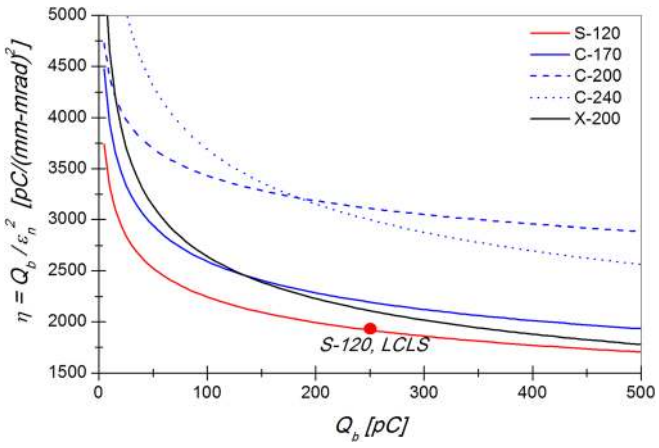

FIG. 2. Optimization of the beam phase space density versus charge for different frequency bands, computed using the optimization code GIOTTO.[14,15] In the legend, S-120, C-170, C-200, C240, X-200 give the RF injector operation value that has been tested (S,C,X bands) and the relative Gun E_z filed peak; the red point on the S-band curve is the LCLS measured value.[16,17]

source requirements, which is $\frac{\Delta\gamma}{\gamma} < 0.1\%$. A solution to meet this energy spread specification, as introduced above, is to inject the electron bunch into the booster Linac with an appropriate bunch length. Considering an on crest operation, in full relativistic conditions, the final beam energy spread is function of the accelerating frequency and bunch length, as shown in the following approximate equation:

$$\frac{\Delta\gamma}{\gamma}_{rms} \approx 2\left(\pi f_{RF}\frac{\sigma_z}{c}\right)^2. \quad (8)$$

Fig. 3 shows the behavior of the relative energy spread as given from Eq. (8) for three different RF accelerating frequencies: X ($\nu_{RF} = 12$ GHz), C ($\nu_{RF} = 6$ GHz), and S ($\nu_{RF} = 3$ GHz). Once an acceptable energy spread has been defined, using both the SPD project requirements and a trade-off of the parameter weighs defining $\frac{\Delta v_\gamma}{v_\gamma}$ (Eq. (4)), the bunch length threshold values are retrieved at the booster entrance, for each different acceleration frequency. It is worth to note that higher accelerating frequencies mean higher beam currents at injection (e.g., for achieving an energy spread lower than 0.05%, representing an ELI-NP safe design value, this would require the following bunch lengths at the booster entrance: $\sigma_z \leq 130\,\mu$m for X-band, $\sigma_z \leq 260\,\mu$m for C-band, and $\sigma_z \leq 520\,\mu$m for S-band).

The operation working point presented here, as result of the optimization and considerations explained previously, is to start at the photocathode with a bunch long enough to control the emittance growth (i.e., avoiding η degradation), due to space charge in the gun region and then to reduce the bunch length by applying the "velocity bunching" technique[18] in the first accelerating section placed after the gun. This technique consists in injecting a not yet relativistic beam in an RF structure with a phase near the zero crossing of the acceleration field: the beam slips back up to the acceleration phase undergoing a quarter of synchrotron oscillation and is chirped and compressed. This concept can be applied to an accelerator based on a hybrid layout, consisting in an S-band photo-injector followed by a C-band Linac that provides a compactness advantage comparing to the full S-band choice. The S-band segment is similar to SPARC: 1.6 cell RF gun with a copper photocathode and an emittance compensation solenoid,[19] followed by two SLAC-type 3 m long travelling wave (TW) sections. A gentle velocity bunching (compression factor < 3) in the first accelerating section allows injecting in to the C-band booster a beam that is short enough to reduce the final energy spread, avoiding emittance degradation. In the first accelerating section, the transverse emittance dilution is controlled by using a solenoid embedding the RF compressor. The velocity bunching technique permits controlling the bunch length, together with the emittance compensation, as routinely done at SPARC. This hybrid solution based on a conservative design of the photo-injector has the advantage to combine a low risk factor with the compactness of a C-band Linac.

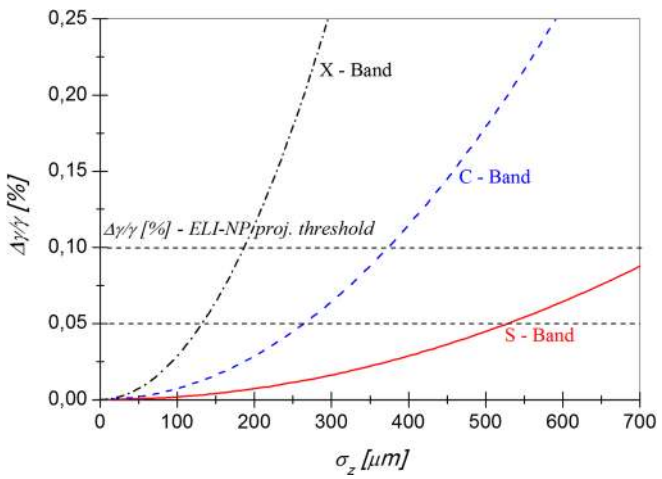

FIG. 3. Energy spread versus bunch length for different RF frequencies: red solid line for the S-band, blue dashed line for C-band, and dashed and dotted black line for X-band. The ELI-NP energy spread maximum threshold is 0.1% and 0.05%; safe values are reported in black dashed lines.

IV. MACHINE LAYOUT

A. The injector

In order to generate a high quality electron beam, according to the criteria discussed above, the operation of the S-band photo-injector for the ELI gamma source has been optimized by extensive computer simulations based on the TSTEP[20] code. This code is an updated version of the macro-particle code PARMELA[21] and is able to take into account the space charge effects, which mainly affect the beam dynamics in this part of the accelerator.

The thermal emittance value utilized in the simulation is 0.9 mm-mrad, a measured value for S-band RF gun operating at 120 MV/m RF peak field.[22] The traveling wave (TW) SLAC type accelerating structures have been set at a gradient of 21 MeV/m, typically employed in the SPARC operations, though a 23–25 MeV/m gradient could be reached. For a good statistic approach, 40 000 macro-particles have been used in the simulation.

A bunch with 0.83 ps (280 μm) length, at the injector exit, as retrieved from the approximated Eq. (8), is required to achieve an energy spread around 0.05% at the end of the C-band Linac. Simulations, with the purpose to maximize the phase space density η of a 280 μm bunch length fixed at the photo-injector end, have explored different operating points, considering a range of 20–500 pC for the electron beam charge. Two of these points are discussed here in detail:

1- a "reference" working point based on a 250 pC electron bunch: the phase space density results maximized and, for this reason, it has been selected for start-to-end simulations, aimed to meet the gamma source requirements;
2- a "commissioning" working point based on a low charge (25 pC) bunch, to be used in the early stages of the machine setup.

In the simulations for these two working points, the starting distributions of the beams are uniform in the transversal plane, which are shaped as shown in Fig. 4 for the longitudinal plane. These shapes minimize the final emittance value.

The plots in Fig. 5 show the details of the computed dynamics of the reference beam, which exits from the photo-

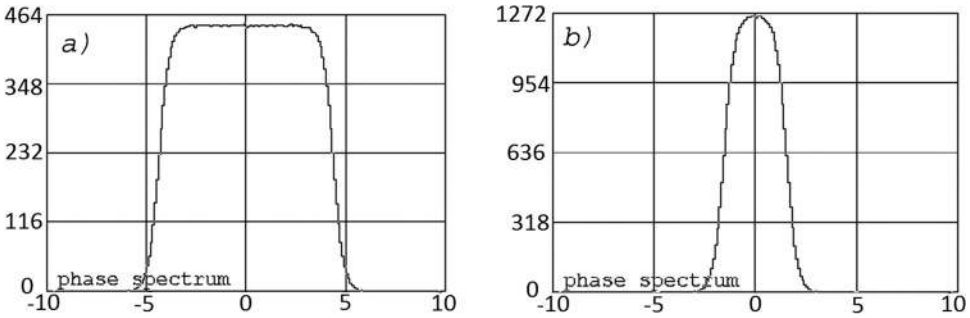

FIG. 4. Photocathode laser pulse shape used in beam dynamic simulations. (a) Reference working point, Q = 250 pC. (b) Commissioning working point, Q = 25 pC.

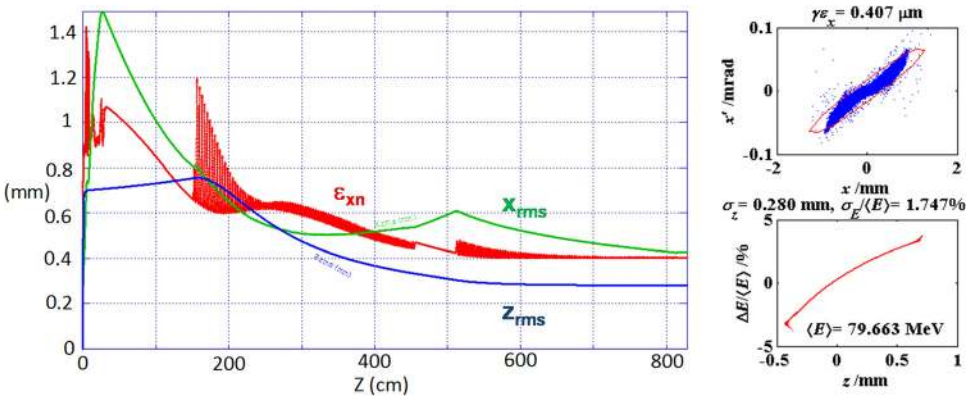

FIG. 5. TSTEP output for the reference working point, Q = 250 pC. (a) Evolution of emittance, transverse and longitudinal envelopes in the S-band photo-injector. (b) Transverse (top) and longitudinal (bottom) phase space at the photo-injector exit.

injector with a projected emittance of 0.4 mm-mrad and with a rms length of 280 μm. This length is achieved by applying a 2.5 RF compression factor. The energy spread induced by the RF compression is recovered working off-crest in the following C-band Linac.

The optimized low charge (25 pC) working point, useful in the commissioning phase and for the machine setup, has been split in two operation modes: with and without RF compression. In the absence of RF compression (first section RF phase on crest), it has been optimized requiring the same bunch length, at injection in the booster, of the reference working point. TSTEP results (see Fig. 6) show how a 280 μm rms length, 0.2 mm-mrad emittance beam is obtained at the photo-injector exit, by operating the first section on crest and with the embedding solenoid switched off, in order to simplify the accelerator initial setting.

In the absence of RF compression, the final energy reaches 131 MeV and the energy spread, for this non-chirped beam, is very low (0.016%), meaning that the off-crest operation in the C-band booster is not needed. If we apply the velocity bunching to this low charge beam, with the same compression factor used for the reference working point, we obtain at the photo-injector exit a beam with a very short bunch length (corresponding, at high energy, to a very low energy spread of 0.01%) and without emittance degradation respect to the "on-crest" operation. The characteristics of these two working points are summarized in Table III.

Following recent experimental results achieved at LCLS,[23] we have also explored a further option potentially able to improve the photocathode gun performance by optimizing the spatial distribution at the cathode. A spatial-cut Gaussian distribution, in the transversal plane, could be more advantageous than the uniform one; which is normally used and obtained by cutting a laser beam with an iris much narrower than the laser itself; this technique causes the loss of laser energy. The LCLS experience points out that the use of a truncated Gaussian laser profile, with a ratio $\sigma_x/r \sim 1$ (σ_x = rms size of the generating Gaussian laser distribution,

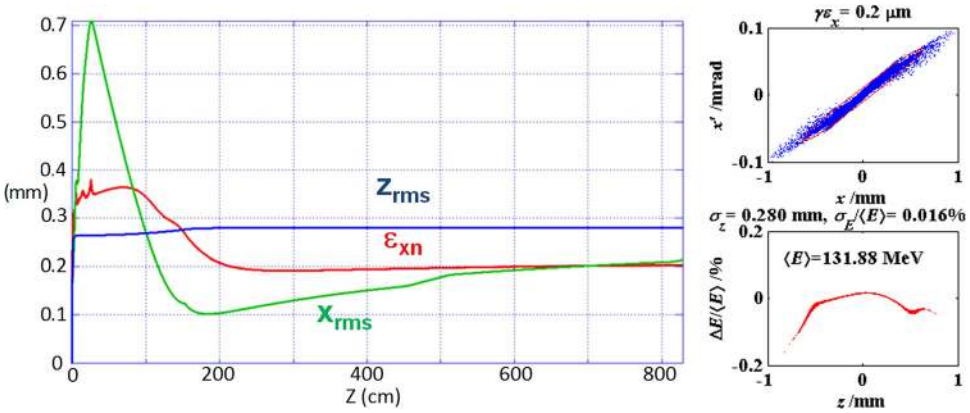

FIG. 6. TSTEP output for the commissioning beam, Q = 25 pC.Operation mode: no RF compression (a) Evolution of emittance, transverse and longitudinal envelopes in the S-band photo-injector. (b) Transverse (top) and longitudinal (bottom) phase space at the photo-injector exit.

TABLE III. Electron beam parameters, at the C-band booster injection, for the S-band photo-injector.

	Reference beam (Comp. factor = 2.5)	Commissioning beam (On crest operation)	Commissioning beam (Comp. factor = 2.5)
Charge (pC)	250	25	25
Laser pulse length @ cathode, FWHM (ps)	8.5	3	3
Photocathode laser rms spot size (μm) (uniform transverse distribution)	250	150	150
Output energy (MeV)	79.7	132	79.6
Output RMS Energy spread (%)	1.75	0.02	0.63
Output normalized RMS projected emittance (mm-mrad)	0.4	0.2	0.2
Output RMS bunch length (μm)	280	280	112

r = iris radius) has two benefits: a significant improvement in laser transmission and an emittance reduction. This last benefit is associated to a more linear behavior of the transverse space charge force for $\sigma_z/r \sim 0.1$ (a condition that usual occurs when the bunch leaves from the cathode). Some beam dynamics simulations have been performed to explore the possibility to improve the ELI-NP photocathode gun operation by using this approach. For the reference 250 pC working point, the uniform spatial distribution used in the simulations discussed above has been compared with a truncated Gaussian spatial profile (Fig. 7) by keeping the same beam diameter on the cathode (1 mm) and optimizing the rms size of the generating laser Gaussian distribution. The longitudinal pulse profile has been kept equal to the optimized shape of Fig. 4.

The rms size of the two distributions in Fig. 8 is very close, being 250 μm and 235 μm; the second one is obtained by truncating a Gaussian distribution with $\sigma_x = 0.4$ mm by using a 0.5 mm radius iris. The effect of the thermal emittance difference is negligible. TSTEP computations show a reduction in the final emittance of about 33% (down to 0.31 mm-mrad) for the truncated Gaussian distribution with respect to the pure uniform one (0.407 mm-mrad) with the same final bunch length (Fig. 8).

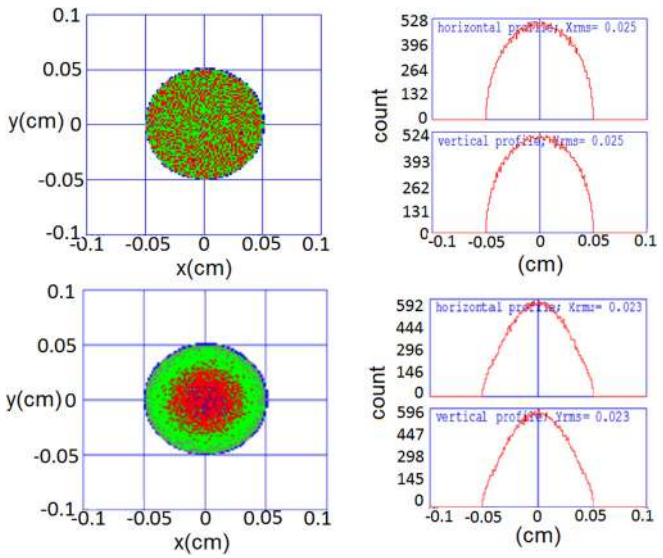

FIG. 7. Initial transverse distributions used into computations. On the top the uniform one, on the bottom the truncated Gaussian one, with $\sigma_x = 0.4$ mm. On the left the spot sizes, on the right horizontal and vertical projections.

This unconventional pulse shaping could significantly improve the quality of the final beam, with the benefit to double, at least, the laser transmission (0.8 instead of 0.4–0.3) through the iris, loosening the required laser power. This power-surplus could also be used to increase the beam charge instead of reducing the emittance. Other simulations have been performed optimizing the beamline parameters (phase and magnetic fields) in order to find the maximum charge value compatible with the same final emittance of the reference 250 pC working point in the case of a Gaussian-cut distribution. As shown in Fig. 9 this upper limit has been found to be 390 pC, with the same bunch length of the reference working point. The differences consist in a small increase of the energy spread and a reduction of the final energy of about 1 MeV (see, for comparison, Fig. 5). This charge gain corresponds to an increase of the gamma-source photon number increase of about 1.6.

All simulations presented here have been performed with a perfect symmetric transverse Gaussian-cut distribution, demonstrating how the overall efficiency could be improved by adopting this spatial laser profile, respect to a uniform one. It is important to stress the fact that in the real operations the emittance improvement could be reduced by transverse beam asymmetries;[24] therefore this option will require a special effort in the commissioning phase to control the laser and cathode uniformity.

B. The booster Linac

The final electron beam energy is reached with a fourteen C-band accelerating sections Linac, downstream of the S-band photo-injector. It is foreseen that these 5.7 GHz C-band sections will operate with an acceleration gradient of 35 MeV/m, bringing the beam up to the maximum energy of 840 MeV (by working on crest). Two beamlines are planned to deliver the electron beam at the two Compton Interaction Points (IPs): one at E = 180–360 MeV and one at E = 500–720 MeV, respectively, the low and the high energy IPs as shown in Fig. 10.

Downstream the photo-injector, a first Linac section (Linac1) with six accelerating structures, is foreseen to bring the electron beam energy up to 360 MeV, and a first dogleg with two branches DL1-L and DL1-H provides on both sides an off axis deviation of 50 cm, avoiding the Bremsstrahlung

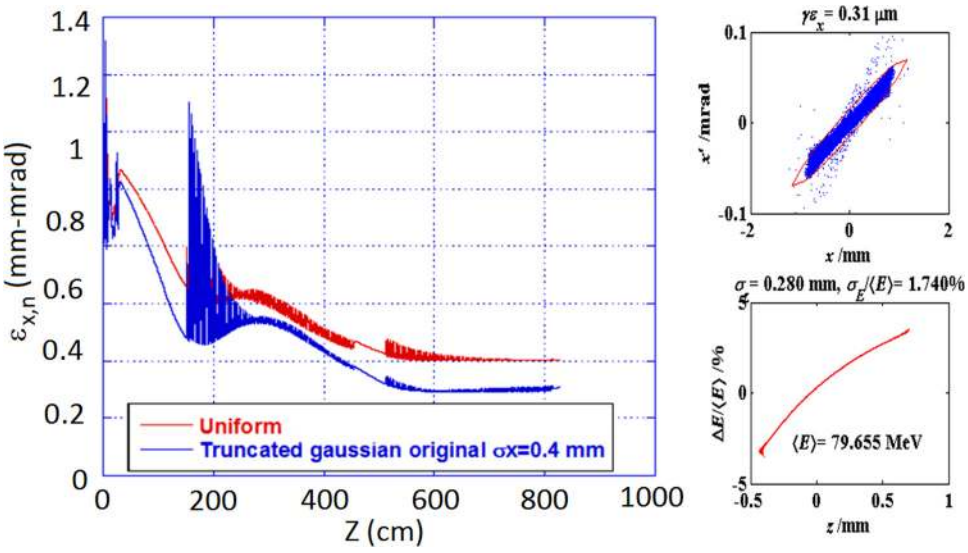

FIG. 8. Q = 250 pC. Left: computed emittance evolution in the ELI S-band photo-injector for a uniform and a truncated Gaussian with $\sigma x = 0.4$ mm. Right: computed output phase space for the truncated Gaussian distribution.

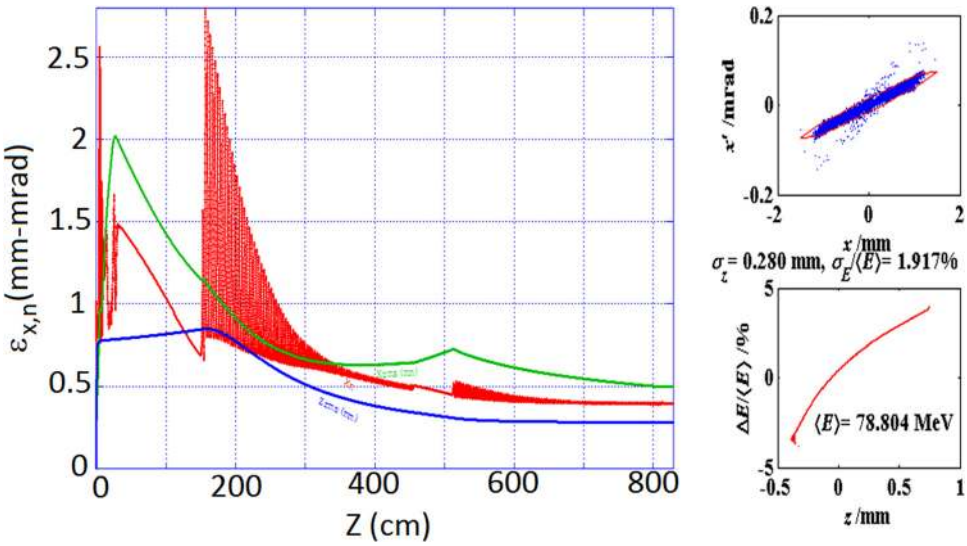

FIG. 9. Q = 390 pC and initial Gaussian truncated distribution with $\sigma x = 0.4$ mm. Left: emittance and envelopes evolution in the S-band photo-injector. Right: Output computed phase spaces.

radiation contribution. The machine operates simultaneously in the two interaction regions: one branch delivers the 360 MeV electron beam to the low energy Compton IP, the other branch brings the electron beam at the entrance of Linac2, where the beam energy is raised up to 720 MeV. A pulsed magnet is foreseen at the dogleg entrance to split up the incoming electron bunches between the IPs. After Linac2, a second dogleg DL2-H drives the beam to the high energy Compton IP, with a further off axis deviation of 1.50 m.

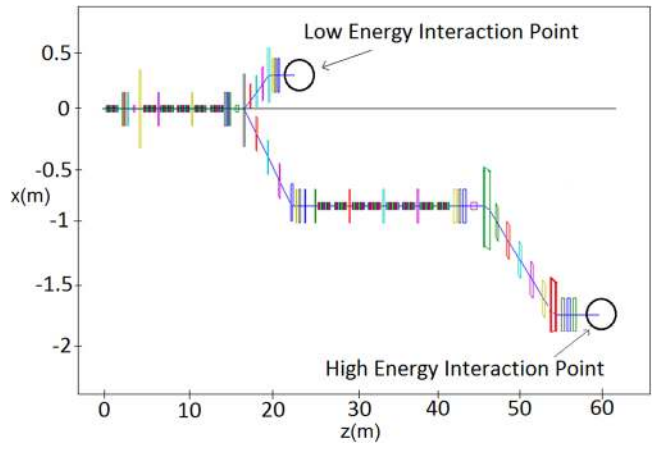

FIG. 10. RF Linac schematic layout from the photo-injector exit down the two interaction points.

A repetition rate of 100 Hz is foreseen together with the possibility of accelerating up to 40 bunches in the same RF pulse with a 15–20 ns spacing to raise the effective rep. rate up to a 3–4 kHz value. The C-band accelerating structure design has been developed at LNF[25] and consists of 85 cells for a total length of L = 1.50 m. A full scale prototype of the structure will be tested and fully characterized with the beam at SPARC (LNF) in spring 2013.

The lattice design of the Linac takes into account a diagnostic section after the first C-band structure, where the electron beam energy is E ~ 120 MeV. This will perform the 6-D phase space characterization just at the exit of the photo-injector by means of an RF-deflector combined with the adjacent spectrometer and of the quadrupole scan technique. After the DL1-L dogleg, a quadrupole triplet provides the electron beam transverse focusing for the interaction with the laser. In Fig. 11, the Twiss parameters of the low energy

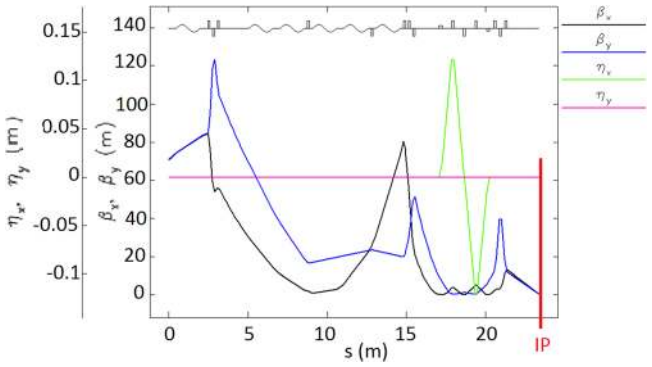

FIG. 11. Twiss parameters of the low energy beamline from the photo-injector exit down to the low energy interaction point.

beamline are reported from the photo-injector exit down to the low energy IP.

The DL1-H dogleg injects the electron beam in the high energy beamline that provides the desired acceleration and focusing for the high energy Compton IP: Fig. 12 shows the high energy beamline Twiss parameters, from the photo-injector exit down to the high energy IP.

The Linac and the transfer lines design have been optimized by extensive numerical simulations performed using the Elegant code,[26] tracking the beam macro-particles obtained with the TSTEP code from the photo-injector exit down to the IPs.

The code takes into account the wake-fields generated by the electron beam inside the accelerating structure together with the coherent and incoherent synchrotron radiation effects in the bending magnets.

For the C-band structure the asymptotic values of the longitudinal and transverse short range wake functions have been calculated according to[27,28]

$$W_{0\|}(s) \approx \frac{Z_0 c}{\pi a^2}\exp\left(-\sqrt{\frac{s}{s_1}}\right)(\mathrm{V/Cm}),$$

$$s_1 = 0.41\frac{a^{1.8} g^{1.6}}{L^{2.4}}$$

$$W_{0\perp}(s) \approx \frac{4Z_0 c s_2}{\pi a^4}\left[1-\left(1+\sqrt{\frac{s}{s_2}}\right)\exp\left(-\sqrt{\frac{s}{s_2}}\right)\right](\mathrm{V/Cm^2}),$$

$$s_2 = 0.17\frac{a^{1.79} g^{0.38}}{L^{1.17}},$$

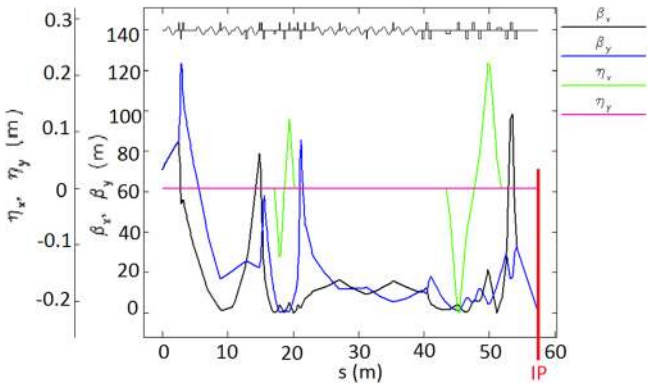

FIG. 12. Twiss parameters of the high energy beamline from the photo-injector exit down to the high energy interaction point.

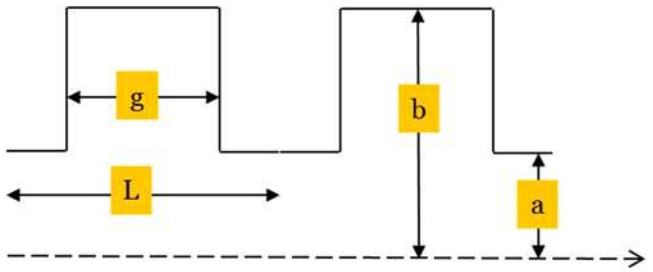

FIG. 13. Pill box cavity model considered for the wake-field calculations: a is the iris radius, L is the cell length, and b and g are the cavity radius and length, respectively.

where Z_0 is the free space impedance, c is the light velocity, a is the iris radius, L is the cell length, b and g are, respectively, the cavity radius and length of the considered pill box model reported in Fig. 13.

The results obtained for the longitudinal and transverse planes are reported in Fig. 14 where they are compared with the results obtained for the SLAC type S-band structures. The Coherent Synchrotron Radiation effect is also taken into account.

The considered electron beam at the exit of the photo-injector, referred as the reference working point, has the following characteristics: charge $Q = 250$ pC, longitudinal rms length $\sigma_z \approx 280\,\mu$m, energy $E \approx 80$ MeV, energy spread $\sigma_\delta \approx 1.8\%$, and transverse normalized emittance $\varepsilon_{\mathrm{n\ x-y}} \approx 0.4\,\mu$ rad (see Table III). The beam simulations computing the travelling of 40 000 macro-particles through the Linac down to the IPs are reported in Table IV.

In Fig. 15 the transverse and longitudinal beam distribution are reported for the two beams, while in Fig. 16 the energy spread and energy distribution are reported together with the current distribution along the bunch.

C. Multi-bunch operation

The challenging characteristic of a very high Spectral Density, as required in gamma-ray sources like ELI-NP, generates the need to operate the machine in a multi-bunch regime, since today this operation method is the only way to reach very high photon fluxes. A rep. rate of 100 Hz for the RF, by injecting 30–40 electron bunches per RF pulse (15–20 ns separated), allows increasing the single interaction photon numbers up to a factor of $4{\cdot}10^3$.

The photoinjector laser will produce a train of UV pulses in order to generate the right amount of charge, once impinging on a copper photocathode. Each pulse will be on the ps range duration, with energies up to 250 μJ, for the highest charge working point. Time structure of the pulse train is conceived in order to properly fill the RF buckets. The photoinjector laser system is a Ti:Sa based laser, diode, and flash pumped, generating an energetic pulse with 100 Hz rep. rate (synchronized with RF macro pulse). Each single pulse, within 100 Hz train will further split by means of an optical cavity, able to be controlled and responded for synchronization purposes. The cavity will supply the micro pulse structure (30–40 pulses with 15–20 ns distance) filling

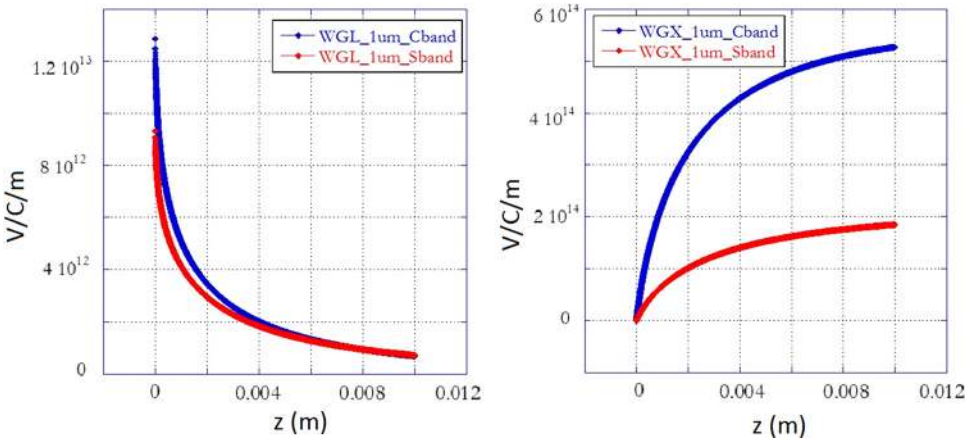

FIG. 14. Longitudinal and transverse short range wake-fields curve integrated over one cell for the S-band accelerating structure (red curve) and for the C-band structure (blue curve).

TABLE IV. Electron beam parameters at the low and high energy interaction point.

	E (MeV)	ε_{nx} (μ-rad)	σ_δ (%)	σ_x (μm)	σ_y (μm)
Low energy IP	360	0.4	0.08	14	14
High energy IP	520–720	0.5	0.05	10	10

the RF buckets within each macropulse. Such a splitting will be operated right before compression of pulses. Ti:Sa bandwidth is used in order to shape quasi flat-top time profile in the pulses. After the amplifier chain, a frequency tripler and a longitudinal/transverse shaping system will deliver the right spot size, duration on cathode. Fast synchronization with respect to the RF system is made at the oscillator level, with a piezo mounted mirror. This technique has shown to guarantee time jitters below 100 fs (RMS).

Long-range wake-fields, in multi-bunch operation, can strongly affect the accelerators beam dynamics. The longitudinal ones, related to the excitation of the fundamental accelerating mode and referred to as beam loading effects, can give an undesired modulation of the beam energy along the bunches train. Several approaches, which are different in case of standing wave (SW) and TW structures, can be found in literature to study and compensate these effects.[29–38] The transverse wake-fields, instead, can drive an instability along the train, which is called multi-bunch beam break up (BBU).[40,41] The BBU, of particular concern in accelerators working with relevant bunch peak current, is excited by off-axis beam trajectories and can rise within a single bunch or along a train of bunches. In our case the main concern is for the multi-bunch operation.

1. Beam loading

The S-band SW 1.6 cell RF gun[39] chosen for the Linac injector, as discussed above, for a multi-bunch train composed by 30–40 of the 250 pC reference bunches (15–20 ns of separation time), shows a negligible voltage induced by the electron beam unlike other photo-injector electron sources that work with higher train currents (e.g., LUCX exp.[40]).

The energy spread generated along the train by beam loading effects in our TW cavities is shown in Fig. 18 (obtained with the analytical expressions of Ref. 30), for constant gradient S-band cavities and for constant impedance C-band cavities, respectively, the injector and the booster of the proposed hybrid Linac. The two curves show both the transient beam loading and the steady state regime. The steady state is noticeably for the C-band structure and it is

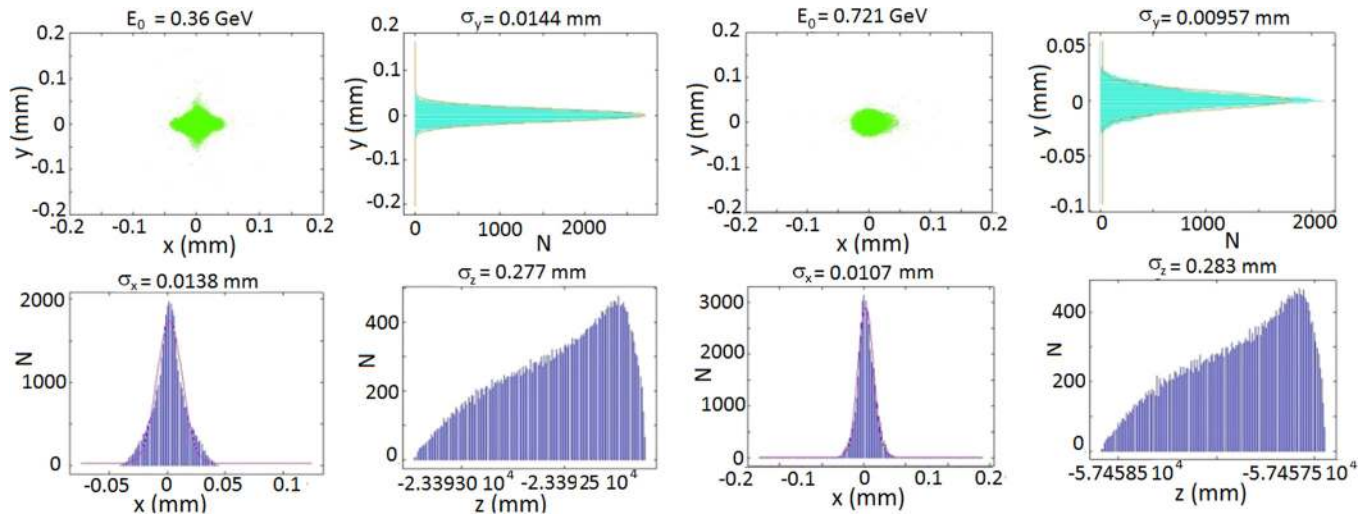

FIG. 15. Transverse beam size and distribution plus the longitudinal one for the reference working point electron beam at the low (left) and high (right) energy interaction point.

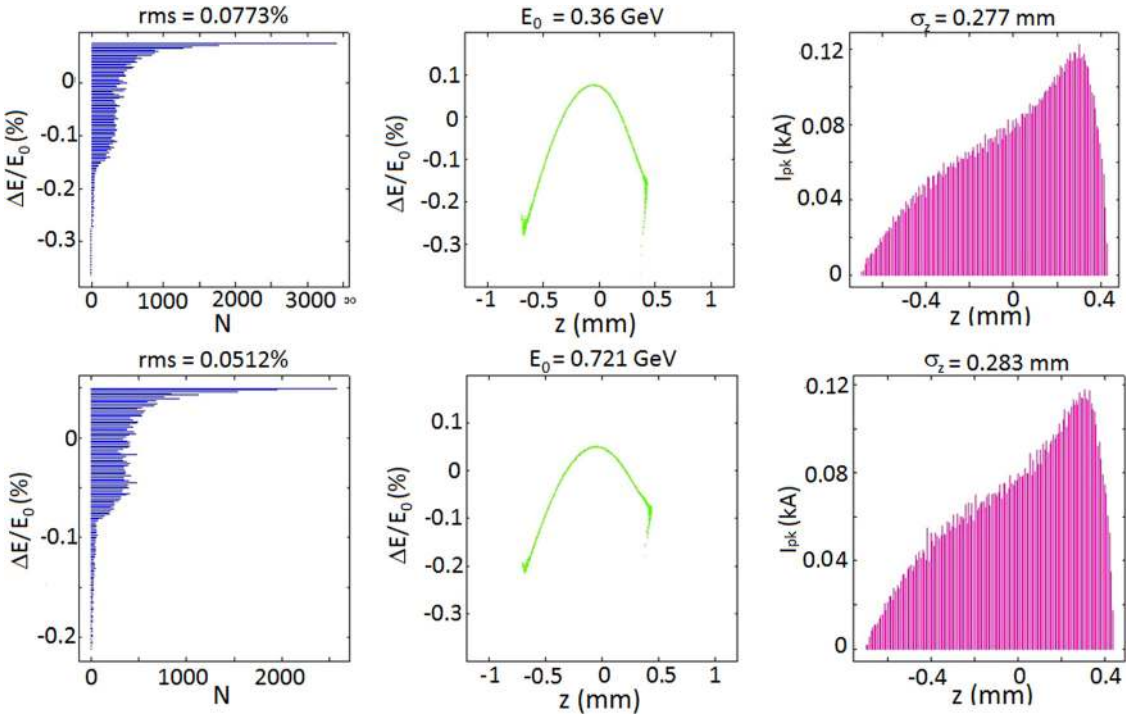

FIG. 16. Beam energy spread, beam energy and beam current distribution of the reference working point at low energy IP (above), and at high energy IP (bottom).

reached when the bunch train is longer than one filling time of the cavity. The results have been obtained with the cavity parameters reported in Table V.

From Fig. 18, it is evident that, if not well compensated, the beam loading effects could produce an unacceptable energy spread along the bunch. There are quite a few techniques to compensate these unwanted effects; some of them are based on a proper modulation of the amplitude and phase of the RF input power,[31–34,36,37] others are based on a proper choice of the beam injection, with respect to the power filling time of the structures.[35]

In our design we have chosen to use the amplitude modulation of the input power along the beam train to compensate the effects, either in SW and TW structures. The correct amplitude modulation of the RF pulse necessary to reduce the energy spread has been calculated and is given in Fig. 17, showing that the beam loading in each cavity can be well compensated (local compensation) such that the induced energy spread is reduced to values much lower than the required ones as shown in Fig. 18. The residual energy spread does not produce any beam dynamics perturbation and induces a tolerable energy modulation at the IPs (Table IV).

TABLE V. Parameters of the TW accelerating structures used in the beam loading calculation.

Parameter	S-band	C-band
Structure type	Constant gradient, TW	Constant impedance, TW
Working frequency	2.856 GHz	5.712 GHz
Structure length	3 m	1.5 m
Nominal RF input power	40 MW	40 MW
Average accelerating	22 MV/m	35 MV/m
Quality factor	13 000	9000
Shunt impedance per unit length	55 MΩ/m	72 MΩ/m
Filling time	850 ns	230 ns

2. Beam break up

Off-axis beam trajectories, source of the BBU effect, arise due to a variety of errors like offset at injection, misalignment of focusing magnets and misalignment of accelerating sections. As a bunch in a beam pulse is displaced from the axis, transverse deflecting dipole modes are excited. The trailing bunches are then deflected by the wake-field forces whether they are on-axis or not. The angular deflections transform into displacements through the transfer matrices of the focusing system and these displaced bunches will create wake-fields in the downstream cavities of the Linac. The subsequent bunches will be further deflected leading to a beam blow-up.

The beam can excite several dipole modes at different frequencies but, in general, the contribution of the dipole modes at the lower frequency dominates. The beam dynamics simulations and the modeling of such phenomena can be done following different approaches.[41–44]

In our case, the most dangerous dipole mode has been evaluated to have a resonant frequency of about 8.4 GHz, a quality factor of 11 000, and R/Q of 0.26 MΩ/m^2. We have then calculated the normalized emittance degradation caused by this transverse wake-field, by using either an analytical approach and by tracking codes which include long range

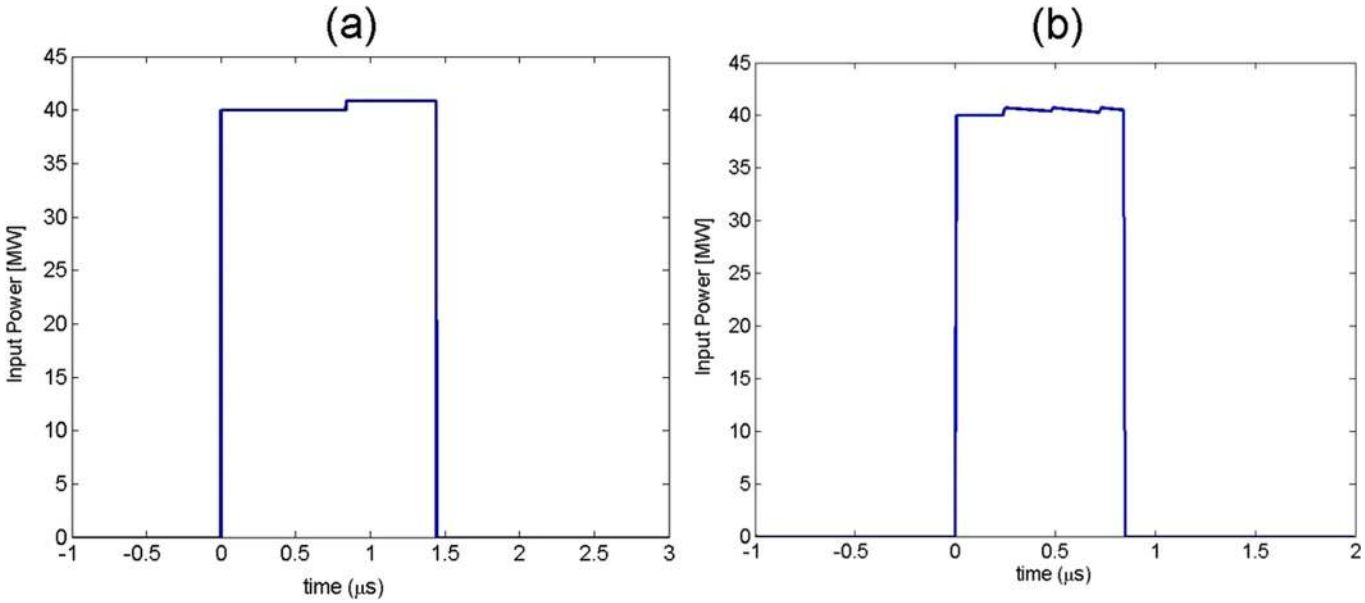

FIG. 17. Input power profiles to compensate the beam loading in the S-band (a) and C-band (b) structures.

wake-fields. By considering a constant β-function along the C-Band Linac and the same dipole mode trapped in each cell of the structure, for a beam misalignment of 100 μm, the result in the emittance increase is of more than a factor ten,[45] which is incompatible with our Linac parameters.

There are several techniques that can be used to solve the BBU problem, depending on the particular application and beam parameters.[46] In some cases it is sufficient to detune the dipole mode from cell to cell, avoiding a complete build up mechanism. In high intensity Linacs nevertheless a strong damping of the dipole mode is often necessary. In our case we have adopted a damping design for the C-band structures (the booster) similar to the X band CLIC (Compact Linear Collider) structures[45–47] designed at CERN, but with a quite lower damping, which is shown in Fig. 19. From electromagnetic simulations performed with GDFIDL,[48] the quality factor of the dangerous dipole mode is reduced to a value less than 100, which in our case is enough to completely remove the BBU effect.

We have also computed the total transverse wake-field for the other two constant gradient S-band structures of the injector, and the result is that the detuning due to the cell variation along the structures is sufficient to avoid in this case the BBU effects.

In conclusion, the multi-bunch effects have been studied using consolidated methods and we believe that we

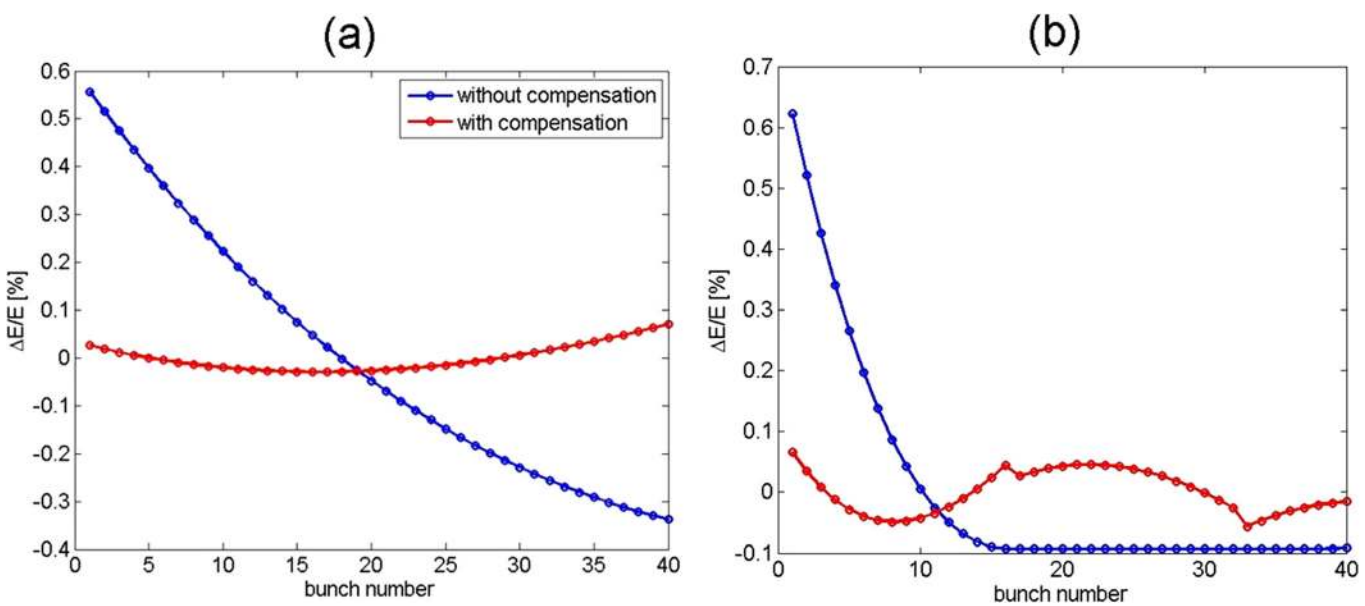

FIG. 18. Energy spread induced by beam loading in the S-band (a) and C-band structures (b) with and without compensation (q = 250 pC, 40 bunches, and $\Delta T = 15$ ns).

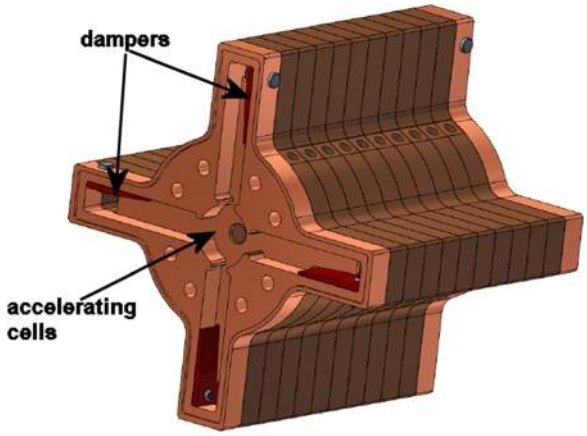

FIG. 19. Mechanical drawing of the C-band damped structure accelerating cells.

have in our design taken sufficient actions to reduce them in order not to constitute an issue for a project like ELI-NP.

V. CONCLUSION

We present a design for an optimized Linac able to meet the challenging requirements of a high-brilliance Compton gamma-ray source, as that foreseen in the context of the ELI-NP facility.

The solution to drive a booster C-band electron Linac, using a 1.6 Cells photo-injector Gun, followed by two S-band SLAC-type traveling wave cavities working with a "soft" velocity bunching technique, as injector, seems to be very promising from more points of view: (1) a very high beam quality given in terms of high electron spectral density into the transverse phase space and low energy spread, (2) a low-risk choice to drive the booster by using a Linac similar to the SPARC[5] one, which is a very consolidated machine and where the velocity bunching technique is routinely successfully used. Further the C-band choice for the booster is a good compromise between acceleration gradient and compactness, and gives the possibility to control beam loading and beam breakup issues in multi-bunch operations.

[1]Ch. Barty, Development of MEGaRay technology at LLNL, http://www.wli-np.ro/executive-comittee-meeting-april-12-13.php and SLAC-PUB-15149 (2012).
[2]H. Toyokawa, Nucl. Instrum. Methods Phys. Res. A **608**, S41–S43 (2009).
[3]H. R. Weller and M. W. Ahmed, Mod. Phys. Lett. A **18**(23), 1569–1590 (2003).
[4]D. Alesini *et al.*, Nucl. Instrum. Methods Phys. Res. A **528**, 586–590 (2004).
[5]S. Ride, E. Esarey, and M. Baine, Phys. Rev. E **52**, 5425 (1995).
[6]W. Brown and F. Hartemann, Phys. Rev. ST– Accel. Beams **7**, 060703 (2004).
[7]P. Tomassini *et al.*, IEEE Trans. Plasma Sci. **36**, 1782 (2008).
[8]P. Oliva *et al.*, Nucl. Instrum. Methods Phys. Res. A **615**, 93 (2010).
[9]M. Bech *et al.*, J. Synchrotron Radiat. **16**, 43 (2009).
[10]W. Brown *et al.*, Phys. Rev. ST– Accel. Beams **7**, 060702 (2004).
[11]V. Petrillo *et al.*, Nucl. Instrum. Methods Phys. Res. A **693**, 109–116 (2012).
[12]D. Alesini *et al.*, in *TUPO008, Proceedings of IPAC2011, San Sebastián, Spain* (2011), pp. 1461–1463.
[13]P. Tomassini *et al.*, Appl. Phys. B: Lasers Opt. **80**, 419–436 (2005).
[14]A. Bacci *et al.*, Nucl. Instrum. Methods Phys. Res. B **263**, 488–496 (2007).
[15]A. Bacci, ULR: http://pcfasci.fisica.unimi.it/Pagine/GIOTTO/GIOTTO.htm.
[16]J. Frisch *et al.*, "Operation and upgrades of the LCLS," in *Proceedings of LINAC'10 Tsukuba, Japan* (2010), p. 694.
[17]P. Emma *et al.*, "Beam brightness measurements in the LCLS injector," Mini-workshop on Compact X-Ray FELs using High Brightness beams, LBNL, 2010.
[18]M. Ferrario *et al.*, Phys. Rev. Lett. **104**, 054801 (2010).
[19]M. Ferrario *et al.*, Phys. Rev. Lett. **99**, 234801 (2007).
[20]L. M. Young, private communication (2009).
[21]L. M. Young, Los Alamos National Laboratory Report LA-UR-96-1835 (1996).
[22]Y. Ding *et al.*, Phys. Rev. Lett. **102**, 254801 (2009).
[23]F. Zhou *et al.*, Phys. Rev. ST Accel. Beams **15**, 090701 (2012).
[24]F. Zhou *et al.*, in *Proceedings of the FEL Conference 2011* (Shangai, China, 2011), p. 341.
[25]D. Alesini *et al.*, "The damped C-band RF structures for the European ELI-NP proposal." Proceeding accepted as contribution at the conference IPA2013, Shanghai China 12–17 May 2013.
[26]M. Borland, "Elegant: A flexible SDDS-compliant code for accelerator simulation," Advanced Photon Source LS-287, September 2000.
[27]K. Bane, "Short-Range Dipole Wakefields in Acc. Struct. For NLC" SLAC-PUB-9663 (2003).
[28]V. Fusco, "Beam dynamics and colective effects in SPARC project" Ph. D. thesis (University La Sapienza, Roma, Italy).
[29]D. Boussard, Beam loading (particle accelerators), CAS—CERN Accelerator School: 5th Advanced Accelerator Physics Course, Rhodes, Greece, 20 Sep–1 Oct 1993, pp.415–436.
[30]J. W. Wang, SLAC Report 339, 1989.
[31]S. Liu *et al.*, Nucl. Instrum. Methods Phys. Res. A **584**, 1–8 (2008).
[32]C. Adolphsen *et al.*, "Beam loading compensation in the NLCTA," in proceedings of PAC 97, Vancouver, 1997.
[33]A. Lunin *et al.*, Phys. Rev. ST. Accel. Beams **14**, 052001 (2011).
[34]O. Kononenko and A. Grudiev, Phys. Rev. ST Accel. Beams **14**, 111001 (2011).
[35]I. Syratchev and T. Higo, KEK Report 96-8, 1996.
[36]M. Satoh *et al.*, Nucl. Instrum. Methods Phys. Res. A **538**, 116–126 (2005).
[37]M. Satoh *et al.*, Phys. Rev. ST Accel. Beams **12**, 013501 (2009).
[38]M. Ferrario *et al.*, Part. Accel. **52**, 1–30 (1996).
[39]D. Palmer, "The next generation photoinjector," Ph.D. dissertation (Stanford University, Stanford, CA, USA, 1998).
[40]A. Deshpande, S. Araki *et al.*, Phys. Rev. ST– Accel. Beams **14**, 063501 (2011).
[41]K. Yokoya, DESY Report No. 86-084, 1989.
[42]Mosnier, in Instabilities in Linacs, CAS—CERN Accelerator School: 5th Advanced Accelerator Physics Course, Rhodes, Greece, 20 September-1 October 1993, pp. 459–514.
[43]D. Schulte, in Proceedings of PAC09, Vancouver, BC, Canada FR5RFP055 (2009).
[44]I. Nesmiyan, IPAC2012/papers/tuppr039.
[45]D. Alesini *et al.*, "Issues for a multi-bunch operation with sparc C-band cavities," in *Proceedings of IPAC2012, New Orleans, Louisiana, USA* (2012), pp. 3042–3044.
[46]R. M. Jones, Phys. Rev. ST Accel. Beams **12**, 104801 (2009).
[47]W. Wuensch, in *Proceedings of the 11th European Particle Accelerator Conference, Genoa, 2008*, EPS-AG, Genoa, Italy, 2008.
[48]See www.gdfidl.de for Software repository, tutorials and manuals.